WATER RESOURCES RESEARCH, VOL. 20, NO. 11, PAGES 1585–1596, NOVEMBER 1984

A Hydrologically Useful Station Precipitation Model 1. Formulation

KONSTANTINE P. GEORGAKAKOS

Hydrologic Research Laboratory, National Weather Service, NOAA, Silver Spring, Maryland

RAFAEL L. BRAS

Department of Civil Engineering, Massachusetts Institute of Technology, Cambridge

A one-dimensional, physically based precipitation model is formulated. Particular emphasis is placed on its utility for real-time river flow forecasting. Thus, the model is in state-space form, suitable for use with modern estimation theory techniques, and it uses only operationally readily available, meteorological variables as its input. Parameterization of the model components is based on well-established observations and theories on water vapor condensation, precipitation mechanisms, and subcloud evaporation of falling hydrometeors. Model input consists of ground level station temperature, pressure, and dew-point temperature observations. The model predicts the spatially averaged, ground surface precipitation rate in the characteristic area determined by the spatial scales of the input. The water equivalent mass condensed in a cloud column defined by the characteristic area is the model state. Key physical parameters in the formulation are the pressure at the cloud top, the height-averaged updraft velocity, and the inverse of the average diameter of the hydrometeors at cloud base.

INTRODUCTION

Rainfall prediction with time leads of the order of hours or, at most, days is the meteorologists' and hydrologists' dream. A prediction would be very valuable in urban hydrology, where basin response is so fast that effective rainfall prediction is the only hope for advanced water resources systems control. In larger, mostly rural basins, a few hours of accurate rainfall input can translate to many more hours of valuable flood warning time. This is best known by the National Weather Service, where stream flow predictions are severely limited by the availability of rainfall predictions at spatial and time scales compatible with their river basin models.

A precipitation model is presented here which takes a first step in satisfying some of the described needs. Model development was directed by the following criteria and objectives:

1. The model should operate at spatial scales of the order of a river basin.
2. It should be able to predict rainfall with at least several hours lead time.
3. It should be simple enough to realistically operate in real time and with reasonable computational needs.
4. The model form should allow updating, given precipitation observations, using modern estimation theory concepts.
5. Model parameters should be clearly related to well-defined physical behavior.
6. Inputs to the model should be easily measured and, preferably, easily forecasted.

This last point is particularly important to the philosophy to be presented, since it is crucial for the development of a model that can be used in real time.

Past attempts at precipitation forecasting using probabilistic or statistical models [*Johnson and Bras*, 1980; *Todini and Bouillot*, 1975] have been of limited success because the rainfall correlation structure is generally quickly decaying. Any linear statistical procedure then has a hard time making predictions. Nevertheless, precipitation is nonlinearly related to a series of meteorological variables, which in turn exhibit slowly decaying correlations and high cross-correlation. Their prediction, using statistical techniques, is then feasible. As will be seen, the precipitation model suggested here will depend on ground station data of temperature (T_0), dew-point temperature (T_d), and ground-level pressure (p_0) as inputs. These are easily measured variables and are presently well predicted by statistical techniques like the model output statistics method of the Techniques Development Laboratory of the National Weather Service [*Glahn and Lowry*, 1972; *Lowry and Glahn*, 1976].

Paper number 4W1075.
0043-1397/84/004W-1075$05.00

MODEL STRUCTURE

Following an old hydrologic concept, the storm cloud system is considered a reservoir of condensed water. During initial development, emphasis will be on a unit area cloud column. Implied spatial dimensions of the development will be discussed later. Figure 1 schematizes the unit area cloud column, moving with horizontal velocity vector u, and defines variables of interest. The center vertical axis of the unit area is represented by coordinate vector $\mathbf{r}$. Vertically, the cloud extends from elevation Z_b to elevation Z_t, where the pressure and temperature are given by p_s, T_s and p_t, T_t, respectively. Ground meteorological conditions are represented by T_0, p_0, and T_d, which were previously defined.

Moisture I is due to the condensation of the vapor carried by incoming air. The state of the cloud is the equivalent liquid moisture content of the column X. A given amount of moisture O_t is blown off the cloud top by updrafts. Outflow at cloud bottom is O_b. The relative amounts of O_t and O_b will depend on the size of hydrometeors and their ability to counteract updraft wind velocity v with their weight. The hydrometeors are distributed in size according to a function $n(D)$, where D is diameter. The cloud bottom output O_b is transformed to precipitation P after suffering a mass reduction due to evaporation of the drops during the trip to ground level.

A conservation of mass statement of the above model definition would be

$$\frac{dX(t)}{dt} = I(t) - O_t(t) - O_b(t) \tag{1}$$

where $X(t)$ is the mass of liquid water equivalent in the con-

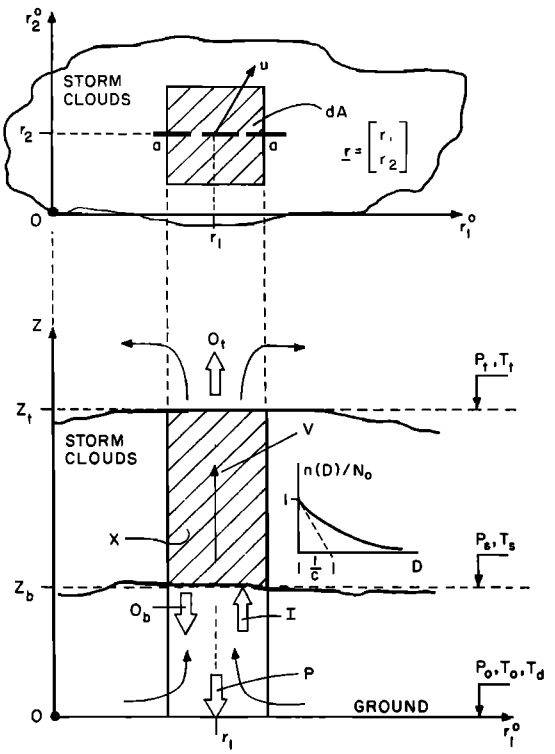

Fig. 1. Schematic representation of the unit area column model variables at time t.

ceptual storage of the unit column; $I(t)$ is the input mass rate due to the condensation of water vapor in the column at time t; $O_t(t)$ and $O_b(t)$ are output values of liquid water as previously discussed. Of interest for hydrological applications is the ground level precipitation rate $P(t)$.

The variables dependence on location r is not shown in order to simplify notation. The task is to define $I(t)$, $O_t(t)$, $O_b(t)$, and $P(t)$ in terms of cloud physics. Because all quantities are implicit functions of time, in the following, dependence on time is not explicitly shown.

Rate of Moisture Input I

The water mass supply of the vertical unit area column is the moisture-laden inflowing air that rises through it. This work assumes conservation of heat of the air masses as they rise. There is no heat exchange between rising air parcels and the ambient air. The parcels are warmed, however, by the release of the latent heat of condensation when they are above the cloud base. The relevant theory is well established in the literature, and pseudo-adiabatic charts have been constructed to facilitate the calculations. It is the purpose of this section to derive an efficient numerical algorithm for the computation of the condensed water mass rate input I.

Assuming that the water content of a volume of air vertically entering the cloud base per unit time will not leave the unit area column from the sides, the input mass rate of condensate is given by

$$I = \Delta w \cdot \rho_m \cdot v \cdot dA \qquad (2)$$

where ρ_m is the vertically (inside the cloud) averaged density of moist air; v is the vertically averaged updraft velocity of inflowing air; dA is the unit area measure; and Δw is the change in specific humidity (approximately equal to the mixing ratio) in the inflowing air between cloud bottom and cloud top; Δw is in grams of moisture per gram of moist air.

The updraft velocity is assumed to vary as in Figure 2, along the vertical, reaching a maximum v_{max} at the elevation where the average of top and bottom pressures occurs. Its values at the cloud top and bottom are equal to a portion β of its vertically averaged value v. The value of v is the value of the updraft velocity at the height defined by the pressure level

$$p_s - \tfrac{1}{4}(p_s - p_t)$$

The updraft velocity is possibly the most important model quantity. As will be seen in a future section, it will be expressed (parameterized) in terms of readily available variables.

Condensation of Water Vapor

Moist, unsaturated air with temperature T_0, pressure p_0, and dew-point temperature T_d is lifted in the storm. As it ascends, it immediately adjusts to the pressure reduction with height and expands. Given that the atmospheric moist air follows closely the ideal gas law, it cools adiabatically. Since the saturation vapor pressure is an increasing function of temperature, and the saturation mixing ratio is an increasing function of the saturation pressure, at some point during its rise the air becomes saturated. This is the lifting condensation level (LCL). Further lifting will result in supersaturated air (supersaturations up to 1% have been observed). However, the excess vapor condenses onto the atmospheric nuclei, suspended in the air, to form minute water or ice particles. Within the storm clouds, the air is saturated with water vapor.

Below the lifting condensation level, the air rises heat-adiabatically with constant potential temperature. Above the level of condensation, the rising air is warmed by the latent heat of condensation, and it is assumed that it follows the pseudo-adiabatic rate, with constant equivalent potential temperature, up to the level of pressure p_t, where the condensation ceases.

It is now necessary to find the mass of liquid water equivalent condensed per unit mass of dry air when an air parcel with initial temperature T_0, initial pressure p_0, and dew-point temperature T_d is lifted up to a terminal pressure level p_t.

The initial mixing ratio w_0 in grams per gram of dry air is

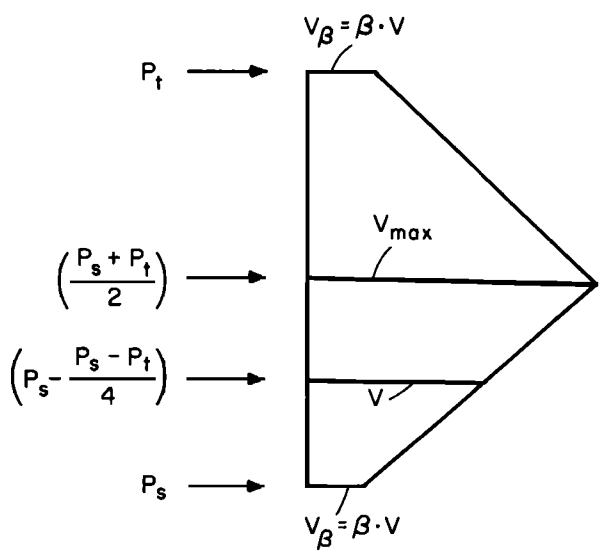

Fig. 2. Updraft velocity variation with pressure: p_s, lifting condensation level pressure; p_t, cloud top pressure; v, height-averaged updraft velocity.

known from the input variables T_d and p_0:

$$w_0 = w_s(T_d, p_0) = 0.622 \frac{e_s(T_d)}{p_0 - e_s(T_d)} \tag{3}$$

where $w_s(T_d, p_0)$ is the saturation mixing ratio at temperature T_d and pressure p_0, and $e_s(T_d)$ is the saturation vapor pressure over a plane surface of pure water.

The saturation vapor pressure e_s is a nonlinear convex function of temperature (solid lines in Figure 3). It is convenient to fit a nonlinear function of the type

$$e_s(T) = A_1 \cdot (T - 223.15)^{3.5} \tag{4}$$

since

$$c_p/R = 3.5$$

where $R = 287$ J kg^{-1} °K^{-1} is the gas constant and c_p is the specific heat at constant pressure ($c_p = 1004$ J kg^{-1} °K^{-1}).

A value of 8×10^{-4} (kg · m^{-1} · s^{-2} · °K$^{-3.5}$) for A_1 gives the fit shown in Figure 3 (dashed line). One can see that equation (4) provides an excellent fit to the observed data [*Mason*, 1971, p. 615] for values of temperature in the range $-30°C \leq T \leq 20°C$ (where a degree Kelvin °K is °C + 273.15).

From (3) and (4) it follows that since $p_0 \gg e_s(T_d)$

$$w_0 \cong 0.622 \cdot \frac{A_1 \cdot (T_d - 223.15)^{3.5}}{p_0} \tag{5}$$

Similarly, the saturation mixing ratio at temperature T_0 and pressure p_0 (i.e., if the air were saturated at T_0) is

$$w_s(T_0, p_0) = 0.622 \cdot \frac{A_1 \cdot (T_0 - 223.15)^{3.5}}{p_0} \tag{6}$$

If $w_0 < w_s(T_0, p_0)$—equivalently, if $T_d < T_0$—the air is not saturated. During the ascent, the temperature and pressure will follow the dry adiabat that originates at T_0, p_0. When the air becomes saturated, the pseudo-adiabat, passing through the level at which saturation was first reached, will be followed for the rest of the ascent.

If $w_0 = w_s(T_0, p_0)$—equivalently, if $T_0 = T_d$—the air is saturated, and pseudo-adiabat will be followed throughout the rising.

During the dry-adiabatic rising, the potential temperature θ of the air stays constant at the value given by the Poisson equation, which implies the following temperature T and pressure p change along a constant temperature θ adiabat [*Wallace and Hobbs*, 1977]

$$T = \left(\frac{1}{p_n^{0.286}}\right) \cdot \theta \cdot p^{0.286} \tag{7}$$

since $R/c_p = 0.286$. The nominal pressure p_n is taken as 10^5 kg m^{-1} s^{-2}.

The dry-adiabatic rising continues until the air parcel becomes saturated. The point (T_s, p_s) where this takes place is the solution of the system of equations (7) and

$$T - 223.15 = \left(\frac{w_0 \cdot p}{A_1 \cdot 0.622}\right)^{0.286} \tag{8}$$

Equation (8) has been inferred from (3) and (4). The system of equations leads to

$$\left(\frac{p_s}{p_n}\right)^{0.286} \left[- \left(\frac{p_n \cdot w_0}{A_1 \cdot 0.622}\right)^{0.286} + \theta \right] = 223.15 \tag{9}$$

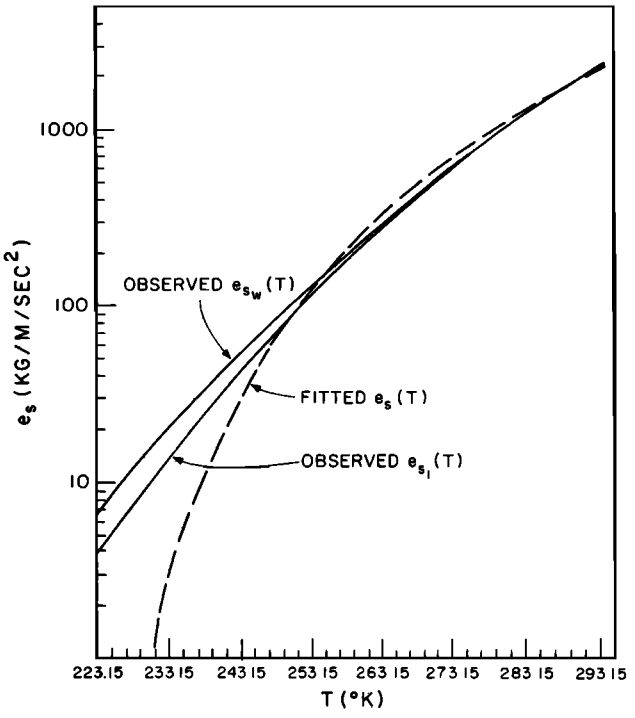

Fig. 3. Observed (solid lines) saturation vapor pressure over a plane surface of water ($e_{s_w}(T)$) or ice ($e_{s_i}(T)$) vs. temperature T. Fitted $e_s(T)$ is dashed line.

By virtue of (5) and (7), with T, p substituted by T_0, p_0, the term in brackets in (9) becomes

$$f_1(T_0, p_0, T_d) = \left(\frac{p_n}{p_0}\right)^{0.286} \cdot (T_0 - T_d + 223.15) \tag{10}$$

By definition, for all values of T_0 and T_d the function f_1, equation (10), is different from zero.

Substitution of (10) in (9), and using the Poisson equation (7), results in

$$\frac{T_s}{T_0} = \left(\frac{p_s}{p_0}\right)^{0.286} = \frac{1}{\left(\frac{T_0 - T_d}{223.15} + 1\right)} \tag{11}$$

So the lifting condensation level (cloud bottom) pressure p_s and temperature T_s are given by

$$p_s = \frac{1}{\left(\frac{T_0 - T_d}{223.15} + 1\right)^{3.5}} \cdot p_0 \tag{12}$$

$$T_s = \frac{1}{\left(\frac{T_0 - T_d}{223.15} + 1\right)} \cdot T_0 \tag{13}$$

It should be noted that the choice of the exponent in (4) is responsible for the simple form of (12) and (13).

Ascent of the air parcel above the level (T_s, p_s) results in the condensation of the water vapor to liquid water. The released latent heat or condensation will warm the air parcel. Consequently, further rising will not be heat adiabatic. It is assumed that the latent heat released does not cross the boundaries of the ascending air mass and that the heat content of the precipitating condensed material is small compared to the heat content of the air mass, so that it does not have to be considered when calculating temperature changes.

Under the above assumptions the characteristic equivalent

potential temperature θ_e of the pseudo-adiabat followed is [*Wallace and Hobbs*, 1977]

$$\theta_e = \theta \cdot \exp\left[\frac{L(T_s) \cdot w_s(T_s, p_s)}{c_p \cdot T_s}\right] \tag{14}$$

where $L(T)$ is the latent heat of condensation, which depends weakly on the temperature. *Eagleson* [1970] suggests a linear function for $L(T)$ of the type

$$L(T) = A - B \cdot (T - 273.15) \tag{15}$$

where $A = 2.5 \times 10^6$ (J kg^{-1}) and $B = 2.38 \times 10^3$ (J kg^{-1} °K^{-1}).

Expressing θ in terms of p and T using (7), and substituting in (14), leads to the following description of the variation of T and p along a constant θ_e pseudo-adiabatic rising

$$\theta_e = T \cdot \left(\frac{p_n}{p}\right)^{0.286} \cdot \exp\left\{\frac{L(T) \cdot w_s(T, p)}{c_p \cdot T}\right\} \tag{16}$$

In the above equation, θ_e is known (by (14)), and the two remaining unknowns are p and T.

Given a terminal pressure level p_t, it is then possible to obtain the corresponding temperature T_t using (16). Furthermore, the final saturation mixing ratio $w_s(T_t, p_t)$ can be computed by an equation of the type in (6). The difference

$$\Delta w = w_0 - w_s(T_t, p_t) \tag{17}$$

is the mass of liquid water resulting from the condensation during the pseudo-adiabatic ascent of a unit mass of dry air. Since the specific humidity q_h is related to the mixing ratio w by $w \cong q_h$ [*Eagleson*, 1970], it follows that Δw is also approximately equal to the mass of liquid water resulting from the ascent of a unit mass of moist air which appears in (2).

Due to the nonlinearity in (16) with respect to the temperature T, Δw cannot be found explicitly. Rather, it must be obtained using numerical iterative methods of root determination (e.g., the Newton-Raphson method). The necessary derivatives and starting value are given in *Georgakakos and Bras* [1982*b*].

In summary the condensed water input can be expressed as

$$I = f(\mathbf{u}, \mathbf{a}_I) \tag{18}$$

where $\mathbf{u}$ is the vector of input variables

$$\mathbf{u}^T = [T_0 p_0 T_d] \tag{19}$$

and $\mathbf{a}_I$ is a parameter vector

$$\mathbf{a}_I{}^T = [p_t v] \tag{20}$$

with the symbol T, when used as a superscript, defining the transpose of a vector or matrix quantity.

An important conclusion is that the input rate I is not (in general) a linear function of the water vapor mass content of the inflowing (in the storm) air.

Discussion of Assumptions in the Unit Area Column Condensation Equation

Due to the large spatial extent and time duration of the storms of significance to hydrologic basins (areas of 1000 km^2), very few (mostly radar-based) observations of the characteristics of the storm dynamics are available (e.g., discussions in *Rogers* [1979]; *Fletcher* [1962]). For the past years, observations of the storm dynamics have been almost exclusively in small-scale convective storms. The discussion of the model assumptions based on these observations is justified by evidence of the existence of convection regions within large-scale stratiform cloud development [*Hobbs and Houze*, 1976; *Fujiwara*, 1976; *Rogers*, 1979].

Observations of the liquid water content of convective clouds by aircraft, summarized by *Byers* [1965], showed that it is significantly less in most cases than the value realized by pseudo-adiabatic parcel ascent. The ratio of observed to theoretical water content ranged from 0.1 for observations on West Indian hurricanes to 0.4 for observations on trade-wind cumulus in the Caribbean, decreasing with height in the cloud. This was explained by the supposition that dry environmental air mixes into the cloud, thus reducing its water content. The extent to which entrainment is important to the types of storm systems of interest in this work cannot be determined on the basis of existing observations. Nevertheless, it can be stated that, if entrainment is important, the model will tend to over estimate the precipitation rate.

Direct deposition from the vapor phase to the solid phase is not taken into account during condensation, therefore, the latent heat of sublimation is not used in Equations (14), (15), and (16). Observations of large numbers of supercooled liquid water droplets at −15°C or colder [*Rogers*, 1979] render this assumption reasonable. Nevertheless, even for very low temperatures, the latent heats of condensation and sublimation differ by less than 10% [*Byers*, 1965].

In using adiabatic transitions it is implicitly assumed that the air below the cloud base is well mixed. That is, the temperature lapse rate is the dry adiabatic and the cloud base is at the lifting condensation level [*Rogers*, 1979]. *Coulman and Warner*'s [1976] aircraft observations in convective clouds indicate that this assumption is reasonable.

Condensation of the water vapor at saturation conditions, not allowing supersaturation, is supported by (1) the presence of hygroscopic nuclei in the atmosphere in vast quantities and sizes and (2) the long time intervals of interest in this work (of the order of a few hours).

The errors due to considering the dry air and the water vapor in moist air as ideal gases are rather small. *Dufour and Defay* [1963] prove that in humid air at pressures less than 1000 [mbar] the error for the dry air is less than 0.1% and the error for the water vapor is less than 1%.

Equation (2) utilizes vertically averaged values of ρ_m and v. Given the uncertainty associated with estimates of v in the unit area column, the increased complexity introduced by integrating over vertically varying updraft velocities and air densities was not considered necessary.

OUTPUT MASS RATE THROUGH CLOUD TOP O_t

The output mass rate per unit area due to the action of the updraft velocity v_β at the top of the cloud, on the smallest water particles with sizes in the interval $(D, D + dD)$, is

$$O_t(D) \cdot dD = \frac{\pi}{6} \cdot \rho_w \cdot D^3 (v_\beta - v_t(D)) n_t(D) \cdot dD \tag{21}$$

with $n_t(D)$ the size distribution at the cloud top, and $v_t(D)$ the terminal velocity of the hydrometeors of diameter D.

The above has to be integrated for the diameter interval $(0, D')$, where D' is the diameter such that $v_\beta \geq v_t(D)$. To perform the necessary integral, the nature of D', which depends on the form of the $v_t(D)$, must be defined. Furthermore, the distribution of particle size $n_t(D)$ at the top of the cloud is required.

Particle Size Distribution $n(D)$

Hydrometeors, or cloud particles, grow in a cloud by a process of condensation and mostly by coalescence, a process

induced by the collision of moving particles [*Eagleson*, 1970]. The distribution of hydrometeor sizes resulting from the growth mechanisms is fairly undefined. Nevertheless, it can be inferred [*Mason*, 1971; *Pruppacher and Klett*, 1978] that the distribution $n(D)$ representing the number of particles of diameter within the interval $(D, D + dD)$ per unit volume of air is such that $n(D)$ increases steeply for D to reach a maximum, and then it decreases with a very mild slope for D.

Several forms for $n(D)$ satisfying the above characteristics have been suggested [*Mason*, 1971; *Pruppacher and Klett*, 1978], but they are all tainted by the difficulties of measuring hydrometeor size in the field. Errors are induced because of (1) inability to measure particles smaller than a given size, (2) inability to measure simultaneously at different locations, and (3) troubles with instrument calibration and reliability under freezing conditions.

Many investigators have then suggested the use of a simple exponential form for the hydrometeor size distribution at a given elevation.

The form (see Figure 4)

$$n(D) = N_0 e^{-cD} \tag{22}$$

has been used by *Marshall and Palmer* [1948], *Gunn and Marshall* [1958], *Dingle and Hardy* [1962], *Ohtake* [1965], *Georgakakos and Bras* [1982*b*] among others. The parameter c in (22) is the inverse mean diameter size at a given level.

The possible objection to (22) is that it implies hydrometeors at diameters approaching zero. The attractive alternative would be to use a distribution starting at zero and peaking somewhere in the small diameter region. Nevertheless, given the acknowledged uncertainties of measuring the number of small hydrometeors, (22) is adequate. In fact the small diameter region plays a small role in the microscopic meteorological and hydrological behavior. For example, the water equivalent mass due to hydrometeors of diameter in the interval $(D, D + dD)$ at a given level (per unit volume) is

$$X(D) = \rho_w n(D) \frac{\pi}{6} D^3 \tag{23}$$

The corresponding rate of mass precipitation out of the cloud would be

$$P(D) = \rho_w n(D) \frac{\pi}{6} D^3 (v_t(D) - v) \tag{24}$$

where ρ_w is liquid water density, $v_t(D)$ is the terminal velocity of a hydrometeor of diameter D, and v is updraft velocity. Assuming (see next section) that

$$v_t(D) = \alpha \cdot D$$

where α is a coefficient, and normalizing (22) by N_0 and (23) and (24) by $\pi\rho_w N_0/6c^3$ and $\pi\rho_w N_0 \alpha/6c^4$, respectively, results in the curves shown in Figure 4.

The normalized size distribution, liquid moisture content, and precipitation rate are given as functions of the nondimensional hydrometeor size measure cD. The obvious result is that most of the moisture and precipitation is due to diameters well above the mean $1/c$. The peak liquid water equivalent occurs at $D = 3/c$ and the maximum water equivalent mass precipitation at $4/c$. Only 1.9% of the total liquid water equivalent mass is contributed by hydrometeors less than $1/c$ in size. The equivalent figure for the precipitated mass rate is 0.37%.

The mean diameter of the hydrometers should be larger near cloud bottom and smaller at the top. This is a reflection

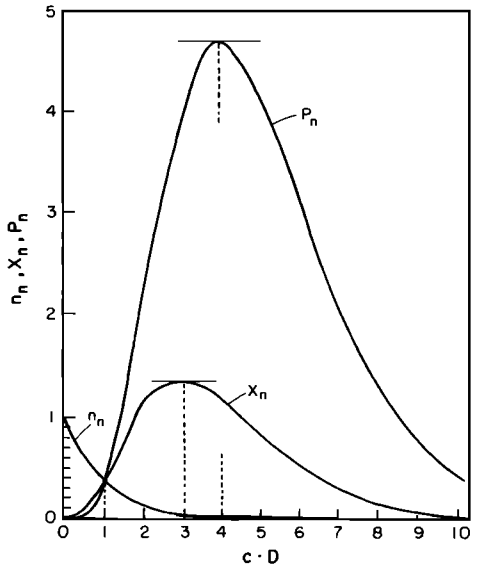

Fig. 4. Normalized number concentration n_n, water mass content X_n, and precipitation rate P_n due to hydrometeors of diameter in the range $(D, D + dD)$ vs. the normalized diameter cD.

of the expected nuclei size distribution and the coalescence mechanism. This distribution is very hard to establish because of the sampling difficulties. A reasonable assumption suggests a simple linear distribution of the value of c with height Z,

$$c(Z) = c_l + \frac{Z}{Z_c}(c_u - c_l) \tag{25}$$

where c_l and c_u are lower and upper values of c, Z_c is the thickness of the cloud column, and Z is height within the cloud measured from cloud bottom.

The mean hydrometeor diameter at a level Z implied by (25) is

$$\bar{D}(Z) = \frac{1}{\left(1 - \frac{Z}{Z_c}\right) \cdot \frac{1}{\bar{D}_l} + \frac{Z}{Z_c} \cdot \frac{1}{\bar{D}_u}} \tag{26}$$

where $\bar{D}_l = 1/c_l$ and $\bar{D}_u = 1/c_u$. The profiles implied by (25) and (26) are shown in Figure 5.

The mass of liquid water equivalent in storage, X, in the column is given by

$$X = \int_0^{Z_t - Z_b} \frac{1}{6} \pi \rho_w N_0 \cdot \left\{ \int_{D_{\min}}^{D_{\max}} D^3 \cdot e^{-D[c_l + (Z/Z_c)(c_u - c_l)]} \cdot dD \right\} \cdot dZ \tag{27}$$

where Z_t, Z_b are the heights of the top and the bottom of the unit area column cloud, and $D_{\min}$, $D_{\max}$ are the minimum and maximum diameters in the cloud.

For $D_{\min}$, $D_{\max}$ taken as 0 and ∞, respectively, (27) gives

$$X = \tfrac{1}{3}\pi\rho_w N_0 Z_c \frac{1}{c_l^4}\left(\frac{c_l}{c_u} + \left(\frac{c_l}{c_u}\right)^2 + \left(\frac{c_l}{c_u}\right)^3\right) \tag{28}$$

Denoting by γ the ratio of the average diameter at cloud base to the average diameter at cloud top, or equivalently,

$$c_u = \gamma \cdot c_l \qquad \gamma \geq 1 \tag{29}$$

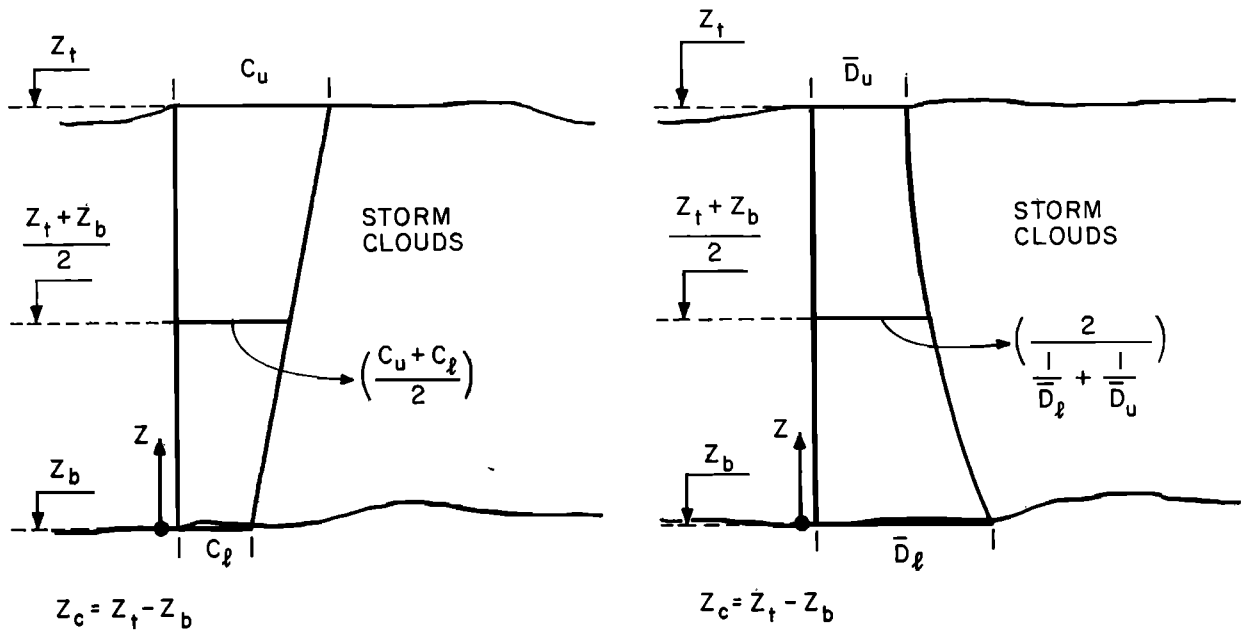

Fig. 5. (*a*) Height variation of the inverse layer-average diameter c: c_u at cloud top and c_l at cloud bottom. (*b*) Height variation of the layer-average diameter $\bar{D}$: $\bar{D}_u$ at cloud top and $\bar{D}_l$ at cloud bottom.

results in

$$X = \pi\rho_w N_0 Z_c \frac{1}{c^4}\left\{\frac{1}{3}\left(\frac{1}{\gamma}+\frac{1}{\gamma^2}+\frac{1}{\gamma^3}\right)\right\} \tag{30}$$

with c_l replaced by c for notational convenience. For a uniform c distribution with height, the result is

$$X = \pi\rho_w N_0 Z_c \frac{1}{c^4} \tag{31}$$

The effect of a linear variation of c with height is the introduction of the factor δ given by

$$\delta = \frac{1}{3}\left(\frac{1}{\gamma}+\frac{1}{\gamma^2}+\frac{1}{\gamma^3}\right) \tag{32}$$

Equation (30) relates the microphysical cloud structure as represented by the parameters N_0, c, and γ to the macrophysical state of the system, the mass X of liquid water equivalent in the unit area column.

From (30), N_0 can be expressed in terms of c as

$$N_0 = \frac{c^4}{\pi\rho_w Z_c \delta} X \tag{33}$$

with corresponding size distribution

$$n(D) = \frac{c^4}{\pi\rho_w Z_c \delta} e^{-cD} X \tag{34}$$

The particle size distribution appearing in (21) is that at the top of the cloud,

$$n_t(D) = \frac{c^4}{\pi\rho_w Z_c \delta} \exp(-c_u D) X \tag{35}$$

Terminal Velocity of Hydrometeors $v_t(D)$

Determining the motion of a particle during free fall in the atmosphere are the gravitational force corrected for buoyancy and the drag force. Due to difficulties in the solution of the Navier-Stokes equations for Reynolds number greater than 1, approximate numerical solutions and field or laboratory observations have been used to determine the terminal velocity of an isolated cloud particle as a function of its size and shape.

Beard [1976] compiled observations of the free fall of liquid water drops of a wide range of diameters (from 1 μ to 7 mm) and presented expressions for the terminal velocity v_t as a function of the diameter D, the particle density ρ_p, and the temperature and pressure, T and p, of the ambient air. Based on Beard's expressions, the terminal velocity of liquid water drops was calculated for a variety of conditions and diameters. For illustration purposes the results for $T = 273.15°K$, $p = 800$ mbar (curve 1) and $T = 293.15°K$, $p = 1013$ mbar (curve 2) are shown in Figure 6. Intermediate conditions lie between the two curves in such a way that v_t decreases as the pressure and temperature increase. This variation of T, p is representative of the conditions expected in the subcloud layer where the precipitation rate is sought. A simple linear approximation to the function $v_t(D)$ is fitted to the results of Beard. It is shown by the dashed line in Figure 6 (curve 3). The fitted curve represents v_t reasonably well for diameters in the range of 1–2 mm, which is the size of most raindrops. It underestimates v_t for diameters in the range of 0.2–1 mm (maximum error less than 20%), and it overestimates v_t for diameters greater than 2 mm. The approximation takes the form

$$v_t(D) = \alpha \cdot D \tag{36}$$

with $\alpha = 3500\ (s^{-1})$.

Contrary to liquid precipitation drops, solid precipitation particles of the same mass display a wide variety of terminal velocities. For the most part this is due to their highly irregular shape. Spherical ice particles of densities 100–900 kg m^{-3} and highly irregular aggregates of dendritic crystals can be found in precipitation. The interested reader is referred to *Magono and Lee* [1966] for a classification of the snow crystals and to *Hobbs et al.* [1974] for a discussion of the dependence of shape and size spectra on the conditions prevailing in the place of formation.

Locatelli and Hobbs [1974] fitted observations of terminal velocity and mass of precipitating solid particles on the Cas-

cade Mountains of Washington state with simple power laws. The scatter of the data is considerable, and no trend was obvious for many classes of shapes.

Figure 6 depicts the regression relationships given in *Locatelli and Hobbs* [1974] for "lump graupel" (curve 5), "hexagonal graupel" (curve 7), and aggregates of dendritic crystals (curve 8). Curves 4 and 6 are *Beard*'s [1976] results for solid spheres of densities 500 and 100 (kg m^{-3}), respectively. The results of *Locatelli and Hobbs* [1974] shown are those for which the regression correlation coefficient was higher than 0.69. The dashed line (curve 9) was "fitted" to all curves corresponding to solid precipitation particles.

The dashed line is a reasonable approximation to conditions found in (1) dendritic aggregates for D in the range 0.5 to 1.5 mm, (2) "graupel" particles for D in the range 1.5 to 2.5 mm, and (3) ice spheres of densities 100–500 kg m^{-3} for D greater than 2.5 mm. For D smaller than 0.5 mm the dashed curve approximates the low-density ice spheres, curve 6, It is expected that the approximation is better than suggested in Figure 6, since the curves of *Locatelli and Hobbs* [1974] correspond to low air density conditions (observations took place at altitudes 750 and 1500 m above sea level). Thus they tend to overestimate the terminal velocities of the snow crystals at lower altitudes.

The dashed line for solid precipitation is of the type in (36) with $\alpha = 1500$ s^{-1}. The terminal velocity of snow particles appears to be about one third that of the liquid water drops with equal mass.

Due to insufficient data in the literature, the velocity of isolated particles is assumed equal to the velocity of a system of particles. Experiments documented in *Sulakvelidze* [1969] show, however, an increase of fall velocity for a system of particles of common dimension as compared to an isolated particle of the same dimension. The increase depends on the distance of the particles expressed in number of diameters, the Reynolds number, and the total number of particles. For Reynolds number of order 10^{-1}, for particle center distances of the order of 15 diameters, the increase is about 25%. As the distance between the particle centers increases, the difference in velocity between the system of particles and a single particle drops rapidly to zero (its value for a distance greater than 30 to 35 diameters). Using the single isolated particle velocity, therefore, would tend to underestimate the precipitation rate, especially during high-intensity periods.

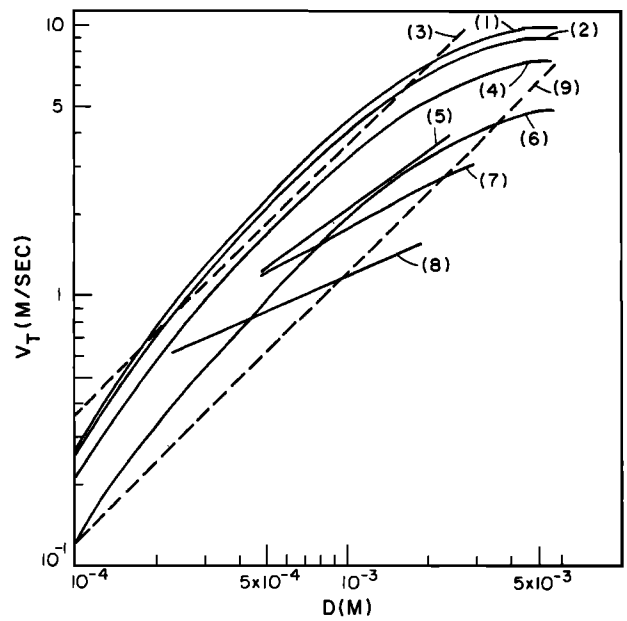

Fig. 6. Observed and fitted terminal velocity as a function of hydrometeor diameter: (curve 1) raindrops, $T = 273.15$°K, $p = 800$ mbar—*Beard* [1976]; (curve 2) raindrops, $T = 293.15$°K, $p = 1013$ mbar—*Beard* [1976]; (curve 3) raindrops, fitted—equation (36); (curve 4) ice sphere, $\rho = 500$ kg/m^3, $T = 273.15$°K, $p = 1013$ mbar—*Beard* [1976]; (curve 5) lump graupel—*Locatelli and Hobbs* [1974]; (curve 6) ice sphere, $\rho = 100$ kg/m^3, $T = 273.15$°K, $p = 1013$ mbar—*Beard* [1976]; (curve 7) hexagonal graupel—*Locatelli and Hobbs* [1974]; (curve 8) aggregates of dendritic crystals—*Locatelli and Hobbs* [1974]; (curve 9) snow, fitted—equation (36).

Determination of the type of precipitation (rain/snow) is based on the surface temperature T_0, such that snow occurs when T_0 is less than 274.50°K [*Eagleson*, 1970].

Summary of Output Mass Rate Through Cloud Top

Having defined the terminal velocity and the particle distribution, it is now possible to integrate the expression for the output mass rate through cloud top, equation (21). The integration is from zero (the smallest particle size) to $D' = v_\beta/\alpha$. Particles of size greater than D' will counteract the cloud top updraft velocity v_β, therefore,

$$O_t = \int_0^{D'} \frac{\pi}{6} \rho_w N_0 D^3 (v_\beta - \alpha D) e^{-c_u D} \, dD \tag{37}$$

where

$$D' = \frac{v_\beta}{\alpha}$$

$$c_u = \gamma \cdot c_l$$

$$N_0 = \frac{c_l^4}{\pi \rho_w Z_c \delta} X$$

Output Mass Rate Through Cloud Bottom, O_b

The output mass rate through cloud bottom is derived similarly to O_t,

$$O_b = \int_{D'}^{\infty} \frac{\pi}{6} \rho_w N_0 D^3 (\alpha D - v_\beta) e^{-c_l D} \, dD \tag{38}$$

where N_0 and D' are similarly defined. The only difference is the use of the c_l value, the inverse of the mean particle diameter at the cloud bottom. The integration is up to ∞, since in principle the particle size distribution admits infinite diameters. In reality a maximum diameter exists. Nevertheless, the exponential decay of the distribution makes the effect of very large particles negligible on the value of O_b.

Surface Precipitation Mass Rate P

Due to evaporation in the subcloud layer, the precipitation rate at ground level is generally only a portion of O_b. Denote P the mass precipitation rate of liquid water equivalent per unit area at ground level. It is given as

$$P = \int_{D_l}^{+\infty} \frac{\pi}{6} \rho_w D^3 \zeta(D) (v_t(D) - v_\beta) n(D) \, dD \tag{39}$$

where the limit D_l is now defined as

$$D_l = \max \left\{ D_c, \frac{v_\beta}{\alpha} \right\} \tag{40}$$

D_c is a critical minimum diameter such that particles of diameter less than D_c will completely evaporate in the sub-

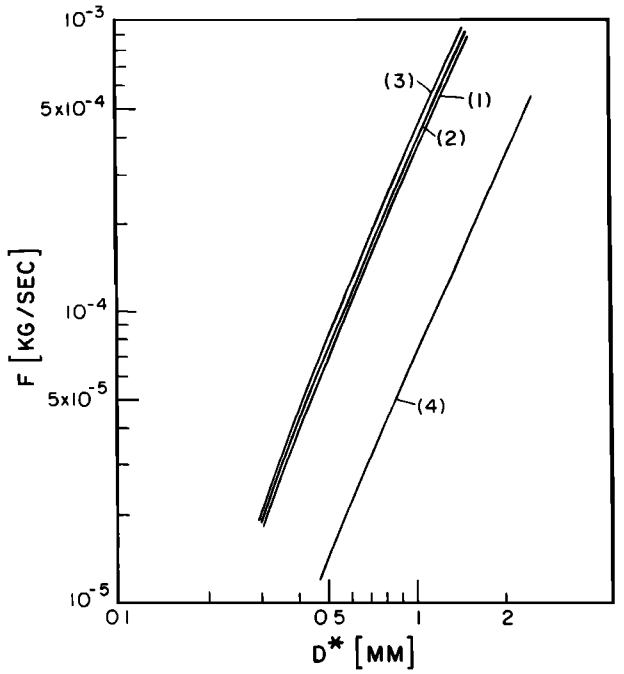

Fig. 7. Integral F as a function of the water equivalent diameter D: (curve 1) $T_0 = 273.15°K$, $p_0 = 1013$ mbar, $\rho_p = 1000$ kg/m^3; (curve 2) $T_0 = 293.15°K$, $p_0 = 1013$ mbar, $\rho_p = 1000$ kg/m^3; (curve 3) $T_0 = 273.15°K$, $p_0 = 800$ mbar, $\rho_p = 1000$ kg/m^3; (curve 4) $T_0 = 273.15°K$, $p_0 = 1013$ mbar, $\rho_p = 100$ kg/m^3.

cloud layer before reaching the ground; $\zeta(D)$ is a function that reduces particle mass. The rate of reduction is a function of the particle diameter. The following subsection defines D_c and $\zeta(D)$.

Evaporation of Precipitating Hydrometeors

Hydrometeors exiting through the cloud base will suffer evaporation throughout their trip to ground level. Evaporation is driven by the difference between the vapor pressure at the particle surface and that in the ambient air. At the particle surface the vapor pressure can be assumed saturated at the wet bulb temperature T_w. In the ambient air the vapor pressure would be equivalent to that at saturation at the dew-point temperature T_d. Since it is expected that $T_w > T_d$, then

$$e_s(T_w) > e_s(T_d)$$

and the vapor pressure gradient is favorable to evaporation. This evaporation is enhanced by the ventilation effect on the particle moving relative to the surrounding air.

According to *Byers* [1965], a motionless droplet with surface temperature T_w loses mass at the following rate:

$$\rho_p D \frac{dD}{dt} = \frac{4D^*}{R_v}\left(\frac{e_s(T_d)}{T_0} - \frac{e_s(T_w)}{T_w}\right) \tag{41}$$

where D is the droplet diameter, t is time, ρ_p is the droplet density, R_v is the gas constant for water vapor (461 J kg^{-1} °K^{-1}), and D^* is the diffusivity of water vapor in air.

Pruppacher and Klett [1978] give the diffusivity as

$$D^* = 2.11 \times 10^{-5}\left(\frac{T_0}{T^*}\right)^{1.94}\left(\frac{p^*}{p_0}\right) \tag{42}$$

where D^* is in m^2 s^{-1} when T^* and p^* take values of 273.15 K and 101,325 kg m^{-1} s^{-2} (1013.25 mbar), respectively. Equation (42) is valid for ambient air temperatures T_0 between 233.15°K (−40°C) and 313.15°K (40°C).

To account for a hydrometeor moving at terminal velocity $v_t(D)$, a ventilation effect factor is introduced in (41):

$$\rho_p D \frac{dD}{dt} = \frac{4D^* f_v(D)}{R_v}\left(\frac{e_s(T_d)}{T_0} - \frac{e_s(T_w)}{T_w}\right) \tag{43}$$

Based on experiments, *Beard and Pruppacher* [1971] suggest the following form for the ventilation factor acting on falling spherical meteors:

$$f_v(D) = \begin{cases} 1 + 0.108\, N_{sc}^{2/3} Re & N_{sc}^{1/3} Re^{1/2} \le 1.4 \\ 0.78 + 0.308\, N_{sc}^{1/3} Re^{1/2} & N_{sc}^{1/3} Re^{1/2} > 1.4 \end{cases} \tag{44}$$

where the Reynold's number Re is defined as

$$Re = \frac{D v_t(D) \rho_a}{\mu} \tag{45}$$

and

$$N_{sc} = \frac{\mu}{\rho_a D^*} \tag{46}$$

In the above equations, ρ_a is the air density at temperature T_0 and pressure p_0 (kg m^{-3}), and μ is the air dynamic viscosity (kg m^{-1} s^{-1}) at temperature T_0. The dynamic viscosity can be obtained by [*Rogers*, 1979]

$$\mu = 1.72 \times 10^{-5}\left(\frac{393}{T_0 + 120}\right)\left(\frac{T_0}{273}\right)^{3/2} \tag{47}$$

where the ambient temperature T_0 is in degrees Kelvin.

For negligible updraft in the subcloud layer the rate change of the hydrometeor position is given by the terminal velocity:

$$\frac{dZ}{dt} = -v_t(D) \tag{48}$$

Using the above in (43) yields an expression in terms of elevation and diameter which in turn can be integrated between a final diameter D_F at elevation 0 and an initial diameter D_0 at the cloud base elevation Z_b:

$$\rho_p \int_{D_f}^{D_0} \frac{D v_t(D)}{f_v(D)}\, dD = \int_0^{Z_b} \frac{4D^*}{R_v}\left(\frac{e_s(T_w)}{T_w} - \frac{e_s(T_d)}{T_0}\right) dZ \tag{49}$$

Figure 7 shows a plot of the integral

$$F(D) = \rho_p \int_0^D \frac{D v_t(D)}{f_v(D)} \cdot dD \tag{50}$$

which appears on the left side of (49). The range of temperatures and pressures cover typical expected values. Notice that curve 4 with 100 kg m^{-3} corresponds to snow (low-density hydrometeors). Clearly, a cubic approximation to (50) is very reasonable,

$$F(D) = C_2 + C_1 D^3 \tag{51}$$

which on substitution in (49) results in

$$C_1(D_0^3 - D_f^3) = \int_0^{Z_b} \frac{4D^*}{R_V}\left(\frac{e_s(T_w)}{T_w} - \frac{e_s(T_d)}{T_0}\right) dZ \tag{52}$$

Georgakakos and Bras [1982*b*] further approximate (52) by assuming that T_w and T_0, as well as pressure conditions, do not change over the elevation to cloud base Z_b. Under the

isothermal and isobaric conditions, (52) becomes

$$D_f^3 = D_0^3 - \frac{1}{C_1}\frac{4D^*}{R_v}\left(\frac{e_s(T_w)}{T_w} - \frac{e_s(T_d)}{T_0}\right) Z_b \tag{53}$$

Notice that (53) can be expressed as

$$\left(\frac{D_f}{D_0}\right)^3 = \zeta(D) \tag{54}$$

with

$$\zeta(D) = 1 - \left(\frac{D_c}{D_0}\right)^3 \tag{55}$$

where D_c is a critical diameter such that particles smaller than D_c completely evaporate on their way to the ground. The critical diameter is

$$D_c = \left[\frac{1}{C_1}\frac{4D^*}{R_v}\left(\frac{e_s(T_w)}{T_w} - \frac{e_s(T_d)}{T_0}\right)Z_b\right]^{1/3} \tag{56}$$

If it is assumed that during a storm $T_w = T_0$, (53) simplifies further,

$$D_f = \left[D_0^3 - \frac{4D^* e_s(T_0)}{C_1 R_v T_0}(1 - r)Z_b\right]^{1/3} \tag{57}$$

where r is the fractional relative humidity

$$r = \frac{e_s(T_d)}{e_s(T_0)}$$

Figure 8 shows the numerical integration of (49) [*Pruppacher and Klett*, 1978] when $D_0 = 1.2$ mm and the relative humidity takes values of 0.6 and 0.8. Elevation zero is taken at cloud base. Given is the travel distance of the hydrometeor. Figure 9 shows similar numerical results [*Beard and Pruppacher*, 1971]. This time the initial diameter is required to end with a 0.2-mm final diameter after a 2000-m fall. The zero level is the ground. Also shown in the figure are the approximations resulting from (57). Figure 9 corresponds to liquid droplets and implies a C_1 value of 7×10^5 kg m^{-3} s^{-1}, which was determined from the fitting of (57) to the results of Figure 8.

The value of C_1 obviously depends on the nature of the hydrometeor. Figure 7 showed the different behavior of snow and liquid precipitation particles. *Georgakakos and Bras* [1982*b*] argued that, if C_2 in (51) is small, then

$$\frac{\text{Rain: } F(D)}{\text{Snow: } F(D)} \approx \frac{\text{Rain: } C_1}{\text{Snow: } C_1}$$

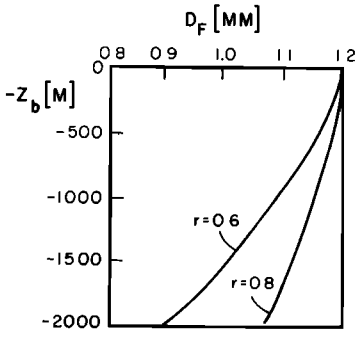

Fig. 8. Numerical integration results in *Pruppacher and Klett* [1978] used to determine the constant C_1 in (57): $T_0 = 278.15$°K and $p_0 = 800$ mbar.

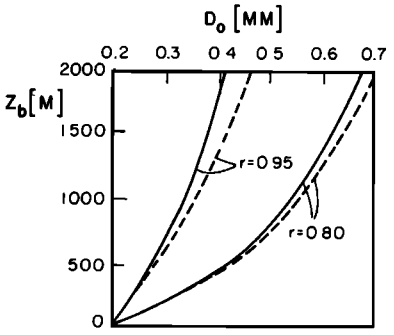

Fig. 9. Initial diameter at cloud base D_0 as a function of Z_b for different values of r. Solid lines are for numerical integration results in *Beard and Pruppacher* [1971]. Dashed lines correspond to (57) with $D_f = 0.2$ mm, $T_0 = 273.15$°K, and $p_0 = 765$ mbar.

From Figure 7 the above ratio is around 5, which implies an approximate C_1 value for snow of 1.4×10^5 kg m^{-3} s^{-1}. Figure 10 gives the critical diameter D_c required for nonzero precipitation as a function of cloud base elevation, relative humidity, and rainfall or snow. The figure results from (56) with $T_w \approx T_0$ and the values of C_1 previously discussed.

Equations (55) and (56) define the factors $\zeta(D)$ and D_c that appear in the precipitation rate and equations (39) and (40).

Summary of Model Equations

Define the dimensionless numbers N_v, N_D, and v_p as

$$N_v = \frac{v_\beta C}{\alpha} \tag{58}$$

$$N_D = cD_c \tag{59}$$

$$v_p = 4\alpha\frac{1}{c} \tag{60}$$

The number N_v is indicative of the updraft strength at the cloud base, since it is the ratio of the diameter (v_β/α) of the particles that possess terminal velocity equal to v_β, to the average diameter $(1/c)$ of the cloud particles. As N_v increases, the updraft strength increases.

The number N_D is a measure of the relative strength of the diffusion process (equation (56)) in the subcloud layer. Diffusion losses increase with increasing N_D.

The velocity v_p corresponds to particles of diameter $(4/c)$, which are the ones that contribute the maximum rate to the total precipitation rate (Figure 4).

Integrating (37), (38), and (39), using the nondimensional numbers just defined, yields

$$O_b = \frac{X}{\delta Z_c} v_p \left[\frac{1 + \frac{3}{4}N_v + \frac{N_v^2}{4} + \frac{N_v^3}{24}}{e^{N_v}}\right] \tag{61}$$

$$O_t = \frac{X}{\delta Z_c} v_p \frac{1}{\gamma^5}\left[\frac{1 + \frac{3}{4}(\gamma N_v) + \frac{(\gamma N_v)^2}{4} + \frac{(\gamma N_v)^3}{24}}{e^{\gamma N_v}} + \frac{\gamma N_v}{4} - 1\right] \tag{62}$$

$$P = \frac{X}{\delta Z_c} v_p \left[\frac{\left(1 - \frac{N_v}{4}\right)\left(1 + N_D + \frac{N_D^2}{2}\right) + \frac{N_D^3}{8}}{e^{N_D}}\right] \tag{63}$$

$$N_D \geq N_v$$

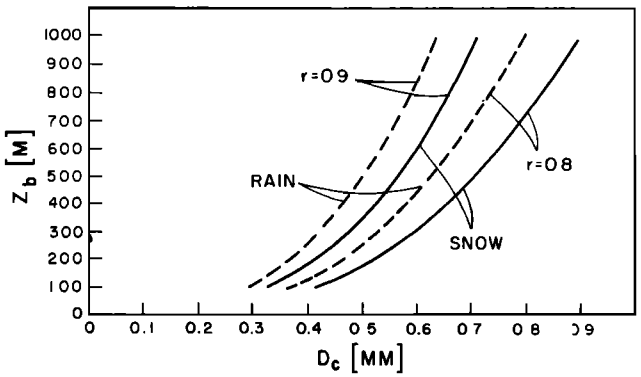

Fig. 10. Initial diameter D_c, at cloud base, of the largest completely evaporating hydrometeor in a subcloud layer of depth Z_b as a function of Z_b for different values of the relative humidity r. For raindrops: $T_0 = 293.15°K$, $p_0 = 1013$ mbar. For snow particles: $T_0 = 273.15°K$, $p_0 = 1013$ mbar, $\rho_p = 100$ kg/m^3.

$$P = \frac{X}{\delta Z_c} v_p \left[\frac{1 + \frac{3}{4} N_v + \frac{N_v^2}{4} + \frac{N_v^3}{24} - \frac{N_D^3}{24}}{e^{N_v}} \right] \quad (64)$$

$$N_v \geq N_D$$

Denote by O_R the reference mass rate per unit area defined by

$$O_R = \frac{X}{\delta Z_c} v_p \quad (65)$$

Then one can define the reduction factors m_b, m_t, and m_p as the ratios of the rates O_b, O_t, and P to the reference rate O_R.

Figure 11 shows plots of m_b, m_t, m_p as functions of N_v, N_D, and γ. Curve 1 represents m_b as a function of N_v. Curves 1, 2, 3 represent m_p as a function of N_v, for N_D equal to 0, 2, and 4, respectively. The reduction factor m_t is represented in curves 4 and 5 for γ equal to 1 and 2, respectively. Based on Figure 11 it can be concluded that

(1) losses through the cloud top (i.e., O_t rate) become significant for $N_v > 3$ if γ is equal to 1 or 2 (The larger the γ, the smaller m_t becomes.);

(2) for low N_D numbers ($N_D < 1$) the precipitation rate that reaches the ground is practically equal to the output rate O_b through the cloud base (curves 1 and 2);

(3) as N_v decreases, the precipitation rate P increases, reaching a maximum as N_v tends to 0 (no updraft at the cloud base); and

(4) for instances of insignificant diffusion losses and for small N_v numbers ($N_v < 0.5$), the precipitation rate P is given by

$$P = \frac{X}{\delta Z_c} v_p \quad (66)$$

Notice that (61) through (64) are linear functions of the state X. The precipitation model equations can then be expressed as

$$\frac{dX}{dt} = f(\mathbf{u}, \mathbf{a}_I) - h(\mathbf{u}, \mathbf{a}_0)X \quad (67)$$

$$P = \Phi(\mathbf{u}, \mathbf{a}_0)X \quad (68)$$

where X is the state, the liquid water content in the cloud; P is precipitation at ground surface; $f(\mathbf{u}, \mathbf{a}_I)$ moisture input; $h(\mathbf{u}, \mathbf{a}_0)$ and $\Phi(\mathbf{u}, \mathbf{a}_0)$ are nonlinear functions clearly defined from (61)–(64). The functions appearing in (67) and (68) are nonlinear in the input vector $\mathbf{u}$ (equation (19)), and in the parameter vectors $\mathbf{a}_I$ and $\mathbf{a}_0$. Vector $\mathbf{a}_I$ was defined in (20), and vector $\mathbf{a}_0$ is defined as

$$\mathbf{a}_0^T = [p_t, v, c] \quad (69)$$

Functions $h(\cdot)$ and $\Phi(\cdot)$ depend on p_t through the appearance in (61)–(64) of $Z_c = Z_t - Z_b$. Assuming hydrostatic pressure in the atmosphere, pressure and elevation are related through the hypsometric equation [*Wallace and Hobbs*, 1977]:

$$Z = \frac{R\bar{T}}{g} \ln\left(\frac{p_0}{p}\right) \quad (70)$$

where $\bar{T}$ is the average temperature in the layer of height Z; R is the dry air gas constant; g is gravitational acceleration, and p_0 is the pressure at the bottom of the layer.

Precipitation as given by (68) is a mass rate per unit area. In order to convert to a depth rate per unit area it is necessary to divide by the density of water.

The linear formulation of (67) and (68) facilitates the use of modern estimation theory concepts in predicting rainfall. Assuming additive errors in the dynamics of moisture in the cloud as well as in the measurement of precipitation, (67) and (68) become

$$\frac{dX}{dt} = f(\mathbf{u}, \mathbf{a}_I, t) - h(\mathbf{u}, \mathbf{a}_0, t)X + \Gamma(t)W(t) \quad (71)$$

$$P = \Phi(\mathbf{u}, \mathbf{a}_0, t)X + V(t) \quad (72)$$

where $W(t)$ is white noise of known variance parameter $Q(t)$ and $V(t)$ is a white-noise sequence of variance $R(t)$. The errors are not cross correlated. The dependence on time has been explicitly shown for the sake of clarity. Equations (71) and (72) exactly fit the format necessary for Kalman filter analysis (continuous dynamics-discrete observations). The unfamiliar reader is referred to one of the many references for details [*Gelb*, 1974; *Schweppe*, 1973; *Georgakakos and Bras*, 1982*b*; *Chiu*, 1978]. The advantage is that the Kalman filter allows the joint processing of the two available information sources: (1) the physically based model dynamics and (2) the observations of precipitation (equation (72)). Since both sources are in error, they are combined according to their reliability to

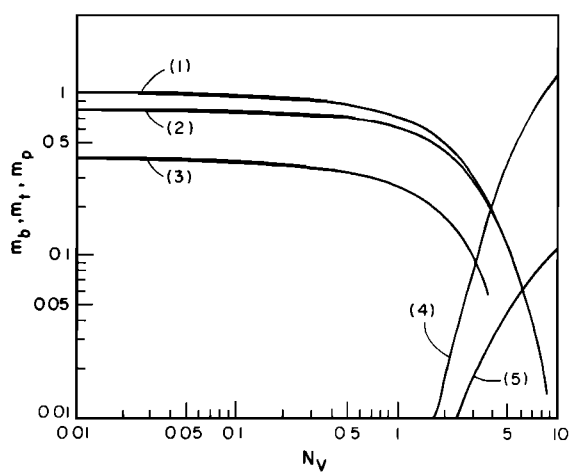

Fig. 11. Reduction factors m_b, m_t, and m_p as functions of the number N_v. N_D and γ are parameters of the plots. Curve 1 is for m_b. Curves 1, 2, and 3 are for m_p and for N_D equal to 0, 2, and 4, respectively. Curves 4 and 5 are for m_t and for γ equal to 1 and 2, respectively.

update the model state $X(t)$ every time an observation of $P(t)$ is available. Forecasting can then be made from updated, better initial conditions.

Given the Kalman filter formulation, the station precipitation model can be used as a stand-alone, real-time rainfall predictor or can be combined with a Kalman filter formulation of a streamflow predicting model [*Kitanidis and Bras*, 1980*a*, *b*; *Georgakakos and Bras*, 1982*a*]. The details of both Kalman filter formulations are given in *Georgakakos and Bras* [1982*b*].

CONCLUSIONS

The rainfall model presented here attempts to cover the important elements of cloud physics that lead to precipitation. The model has several advantages:

1. It results in linear equations of the state, here defined as the cloud moisture content.
2. The inputs to the model are measured at ground level, they are temperature T_0, dew-point temperature T_d, and pressure p_0.
3. Although the model is based on a unit area column developed for point precipitation, it is reasonable for scales comparable to the size and time response of river basins. The spatial and time scales will be fixed by the rate of variation in space and time of the inputs T_0, T_d, and p_0. As it will be seen in an accompanying paper [*Georgakakos and Bras*, 1984], these variables exhibit very high correlation in time and space.

As it stands, the model parameters are p_t, v, and c. These parameters are not necessarily easy to obtain. In concept, p_t is available from remote sensing or radiosonde information. It is also possible to obtain the updraft velocity from similar sources [*Ingraham and Russel*, 1981]. The particle size distribution parameter c is location dependent and would have to be fixed from literature or calibrated.

The above parameter sources are not convenient and are unavailable in many locations. Furthermore, they will vary from storm to storm and within a storm, making real time monitoring absolutely necessary. An alternative is to parameterize p_t, v, and c in terms of other more accessible meteorological variables. In an accompanying paper [*Georgakakos and Bras*, 1984] the authors do just that. Model behavior is tested there with real storms in different locations and climates. The model is also compared to simpler statistical approaches. The results are quite satisfactory.

Acknowledgments. This work was sponsored by the Department of Commerce, National Weather Service, Hydrologic Research Laboratory, under contract NA80AA-H-00044. Work was performed at the Ralph M. Parsons Laboratory, Department of Civil Engineering, Massachusetts Institute of Technology, and at the Hydrologic Research Laboratory, National Weather Service, NOAA. The National Research Council sponsored Georgakakos' work at HRL as an NRC-NOAA research associate. During the preparation of this document, Bras was partly supported by the John Simon Guggenheim Foundation and Simon Bolivar University, Caracas, Venezuela. The authors acknowledge the commentary of Peter S. Eagleson, John L. Wilson, and Michael D. Hudlow. We want to thank Alonso Rhenals and two other anonymous reviewers for their quick response in an unusual situation.

REFERENCES

Beard, K. V., Terminal velocity and shape of cloud and precipitation drops aloft, *J. Atmos. Sci.*, *33*, 851–864, 1976.

Beard, K. V., and H. R. Pruppacher, A wind tunnel investigation of the rate of evaporation of small water drops falling at terminal velocity in air, *J. Atmos. Sci.*, *28*, 1455–1464, 1971.

Byers, H. R., *Elements of Cloud Physics*, The University of Chicago Press, Chicago, Ill., 1965.

Chiu, C. L. (Ed.), Applications of Kalman Filter to Hydrology, Hydraulics and Water Resources, Proceedings of AGU Chapman Conference, Dep. Civil Eng., Univ. Pittsburgh, Pittsburgh, Pa., 1978.

Coulman, C. E., and J. Warner, Aircraft observations in the subcloud layer over land, paper presented at International Cloud Physics Conference, Am. Meterol. Soc., Boulder, Colo. July 26–30, 1976.

Dingle, A. N., and K. R. Hardy, The description of rain by means of sequential raindrop-size distributions, *Publ. 59*, Meteorol. Lab., Univ. Mich., Ann Arbor, Mich., 1962.

Dufour, L., and R. Defay, *Thermodynamics of Clouds*, translated by M. Smyth and A. Beer, Academic, New York, 1963.

Eagleson, P. S., *Dynamic Hydrology*, McGraw-Hill, New York, 1970.

Fletcher, N. H., *The Physics of Rainclouds*, Cambridge University Press, New York, 1962.

Fujiwara, M., A cloud structure and the rain efficiency as observed by radars and raindrop recorder, paper presented at International Cloud Physics Conference, Am. Meteorol. Soc., Boulder, Colo. July 26–30, 1976.

Gelb, A. (Ed.), *Applied Optimal Estimation*, The MIT Press, Cambridge, Mass., 1974.

Georgakakos, K. P., and R. L. Bras, Real time, statistically linearized adaptive flood routing, *Water Resour. Res.*, *18*(3), 513–524, 1982*a*.

Georgakakos, K. P., and R. L. Bras A precipitation model and its use in real-time river flow forecasting, *Tech. Rep.*, *286*, Ralph M. Parsons Lab., Hydrol. Water Resour. Syst., Dep. Civil Eng., Mass. Inst. Technol., Cambridge, Mass., 1982*b*.

Georgakakos, K. P., and R. L. Bras, A hydrologically useful station precipitation model, 2, Case studies, *Water Resour. Res.*, this issue.

Glahn, H. R., and D. A. Lowry, The use of model output statistics (MOS) in objective weather forecasting, *J. Appl. Meteorol.*, *11*, 1203–1211, 1972.

Gunn, K. L. S., and J. S. Marshall, The distribution with size of aggregate snowflakes, *J. Meteorol.*, *15*, 452–461, 1958.

Hobbs, P. V., and R. A. Houze, Jr., Mesoscale structure of precipitation in extratropical cyclones, paper presented at International Cloud Physics Conference, Am. Meteorol. Soc., Boulder, Colo., July 26–30, 1976.

Hobbs, P. V., S. Chang, and J. D. Locatelli, The dimensions and aggregation of ice crystals in natural clouds, *J. Geophys. Res.*, *79*(15), 2199–2206, 1974.

Ingraham, D. V., and S. O. Russell, Nowcasting areal rainfall over British Columbia from GOES satellite images, paper presented at the International Symposium on Real-Time Operation of Hydrosystems, World Meteorol. Org., Univ. Waterloo, Ontario, June 24–26, 1981.

Johnson, E. R., and R. L. Bras, Multivariate short-term rainfall prediction, *Water Resour. Res.*, *16*(1), 173–185, 1980.

Kitanidis, P. K., and R. L. Bras, Real-time forecasting with a conceptual hydrologic model, 1, Analysis of uncertainty, *Water Resour. Res.*, *16*(6), 1025–1033, 1980*a*.

Kitanidis, P. K., and R. L. Bras, Real-time forecasting with a conceptual hydrologic model, 2, Applications and results, *Water Resour. Res.*, *16*(6), 1034–1044, 1980*b*.

Locatelli, J. D., and P. V. Hobbs, Fall speeds and masses of some precipitation particles, *J. Geophys. Res.*, *79*(15), 2185–2197, 1974.

Lowry, D. A., and H. R. Glahn, An operational model for forecasting probability of precipitation—PEATMOS PoP, *Mon. Weather Rev.*, *104*, 221–232, 1976.

Magono, C., and C. W. Lee, Meteorological classification of natural snow crystals, *J. Fac. Sci., Hokkaido Univ.*, *7*(2), 321, 1966.

Marshall, J. S., and W. McK. Palmer, The distribution of raindrops with size, *J. Meteorol.*, *5*, 165–166, 1948.

Mason, B. J., *The Physics of Clouds*, 2nd ed., Clarendon, Oxford, 1971.

Ohtake, T., Preliminary observations of size distribution of snowflakes and raindrops at just above and below the melting layer, paper presented at International Conference on Cloud Physics, World Meteorol. Org., Tokyo and Sapporo, Japan, May 24 to June 1, 1965.

Pruppacher, H. R., and J. D. Klett, *Microphysics of Clouds and Precipitation*, D. Reidel, Boston, Mass., 1978.

Rogers, R. R., *A Short Course in Cloud Physics*, 2nd ed., Pergamon, New York, 1979.

Schweppe, F., *Uncertain Dynamic Systems*, Prentice Hall, Englewood Cliffs, N. J., 1973.

Sulakvelidze, G. K., *Rainstorms and Hail*, translated from Russian by Israel Program for Scientific Translations, Jerusalem, 1969.

Todini, E., and D. Bouillot, A rainfall-runoff Kalman filter model, in *System Simulation in Water Resources*, edited by G. C. Vansteenkiste, North-Holland, Amsterdam, 1975.

Wallace, J. M., and P. V. Hobbs, *Atmospheric Science, An Introductory Survey*, Academic, New York, 1977.

R. L. Bras, Department of Civil Engineering, Massachusetts Institute of Technology, Cambridge, MA 02139.

K. P. Georgakakos, Hydrologic Research Laboratory, National Weather Service, NOAA, Silver Spring, MD 20910.

(Received October 21, 1983;
revised July 31, 1984;
accepted August 1, 1984.)